Environmental Technology & Innovation 24 (2021) 102078

Contents lists available at ScienceDirect

Environmental Technology & Innovation

journal homepage: www.elsevier.com/locate/eti

Interactions between zinc oxide nanoparticles and hexabromocyclododecane in simulated waters

Anwar Ul Haq Khan [a,b], Yanju Liu [a,b,*], Ravi Naidu [a,b], Cheng Fang [a,b], Raja Dharmarajan [a,b], Hokyong Shon [c]

[a] Global Centre for Environmental Remediation (GCER), College of Engineering Science and Environment, The University of Newcastle (UON), Callaghan, NSW 2308, Australia
[b] Cooperative Research Centre for Contamination Assessment and Remediation of the Environment (CRC CARE), ATC Building, The University of Newcastle (UON), Callaghan, NSW 2308, Australia
[c] School of Civil and Environmental Engineering, University of Technology Sydney (UTS), City Campus, Broadway, NSW 2007, Australia

ARTICLE INFO

Article history:
Received 12 June 2021
Received in revised form 28 October 2021
Accepted 30 October 2021
Available online 2 November 2021

Keywords:
ZnO-NPs
HBCD
Zeta potential
Agglomeration
Aqueous media

ABSTRACT

The zinc oxide nanoparticles (ZnO-NPs) have been increasingly applied in industries and consumer products, causing release of these nanoparticles in environments. The behaviour of ZnO-NPs in the water systems is complicated due to the presence of different cations, anions, organic substances (e.g. humic acid HA) and other organic pollutants (e.g. commonly used brominated flame retardant, BFR). In particular, the aggregation and alteration of these nanoparticles can be influenced by co-existence contaminants. In this study, the interactions between hexabromocyclododecane (HBCD) and ZnO-NPs were investigated for the physicochemical properties and colloidal stability changes in various simulated waters. This is significant to understand the fate and behaviour of ZnO-NPs at environmental relevant conditions. The surface chemistry and particle size distribution (PSD) of ZnO-NPs with and without the existence of HBCD, HA and electrolytes (NaCl, $CaCl_2$ and $MgCl_2$) after different periods (1 and 3 weeks) were investigated at pH 7.00 $\pm$ 0.02. The size of the ZnO-NPs increased from nanometres to micrometres with the addition of numerous concentrations of HBCD, HA, and cations and their mixtures. The zeta potential of ZnO-NPs increased upon addition of HBCD, HA and electrolytes indicating a more stable agglomeration form while less agglomeration was observed in the ZnO-NPs and HA suspension after 3 weeks. Hydrophobic and electrostatic interactions, van der Waals forces, including hydrogen bonding and cation bridging could be potential interactive driving forces. The results indicated agglomeration of ZnO-NPs in the existence of organic substances, salts and contaminants, thus sedimentation and precipitation are promising under salty surface water/sea water.

1. Introduction

Engineered nanoparticles (ENPs) are chemically synthesised nanoparticles. ENPs have size range from 1 to 100 nm (Quigg et al., 2013), and are largely employed in agriculture, the environment and consumer products (Sharma et al., 2019;

* Corresponding author at: Global Centre for Environmental Remediation (GCER), College of Engineering Science and Environment, The University of Newcastle (UON), Callaghan, NSW 2308, Australia; Cooperative Research Centre for Contamination Assessment and Remediation of the Environment (CRC CARE), ATC Building, The University of Newcastle (UON), Callaghan, NSW 2308, Australia.
E-mail address: yanju.liu@newcastle.edu.au (Y. Liu).

https://doi.org/10.1016/j.eti.2021.102078

Wang et al., 2013). The zinc oxide NPs are among the top five highly synthesised and employed ENPs in the fast-growing nanotechnology market (Leareng et al., 2020). ZnO-NPs have largely been integrated in the products, such as cosmetics, nanomedicines, plastics, sunscreens, textiles, UV filters and paints and coatings (Caballero-Guzman and Nowack, 2016; Leareng et al., 2020; McCall et al., 2018; Schneider and Lim, 2019). An estimated worldwide annual production of 550-33,400 tons/year of ZnO-NPs make them extensively employed metal-based nanoparticles (Peng et al., 2017; Rajput et al., 2018), and a considerable fraction of the products ends up in natural aquatic systems annually. Many reports have documented the existence of ENPs in environmental samples and wastewater treatment plants (Bundschuh et al., 2018; Nowack and Bucheli, 2007; Park et al., 2017; Westerhoff et al., 2011). It is documented that zinc oxide nanoparticles concentrations in soils and waters are from 3.1 to 31 μg/kg and from 76 to 760 μg/L respectively (Ghosh et al., 2016; Rajput et al., 2018), which are normal to rise with time because of continuous rise in the usage of these nanoparticles (Song et al., 2017). A survey focusing on wastewater treatment plants showed that the yearly average amounts of ZnO-NPs captured by primary sludge particulates and secondary sludge particulates were equivalent to 7.1 kg-ZnO/d and 8.9 kg-ZnO/d, respectively (Choi et al., 2018).

The ZnO-NPs post usage in consumer products could pose negative influences on the environment (Ali et al., 2012; Falfushynska et al., 2015; Gagné et al., 2019, 2015; Khan et al., 2019; Wong et al., 2020; Yi et al., 2018). For instance, ZnO-NPs toxic effects in the marine organisms have also been reported. It is stated that the exposure of ZnO-NPs (i.e 10 and 50 mg/L) in the aqueous media plays a significant role in oxidative stress induction, cytotoxicity, haemocytes genotoxicity, histological mutations in the gills and digestive glands of fresh water (*C.* aegyptiaca) mussel (Fahmy and Sayed, 2017). A similar study also reported on the oxidative stress and genotoxicity caused by ZnO-NPs in snail *Lymnaea luteola L.* in freshwaters (Ali et al., 2012). Due to ease of ZnO-NPs dissolution, the released zinc ions (Zn^{2+}) would largely participate to their toxicity. It is illustrated that the transmembrane ZnO-NPs elevated the intracellular total Zinc (Zn), because of the interaction between algae and zinc oxide nanoparticles, which ultimately brought about the microalgae production repression (Ahamed et al., 2021; Zhang et al., 2016). Zinc oxide NPs aggregate in water systems are also responsible of cytotoxicity in green algae (Ahamed et al., 2021).

Thus, it is significant to know the behaviour and mobility of zinc oxide NPs in wet environment to facilitate the risk assessment. The zinc oxide NPs colloidal stability and toxicity could be altered by numerous environmental factors including extracellular polymeric materials, vital particle size, dissolved organic matter (DOM), ionic strength and pH. Studies revealed that ZnO-NPs are not stable in high ionic strength aqueous media such as seawaters and DOM could altered their colloidal stability (Khan et al., 2019). Increased agglomeration and decreased dissolution of virgin ZnO-NPs in water systems have been observed for pH values approaching to zero point of charge. More agglomeration of zinc oxide NPs has been observed in low fluvic acid to ZnO-NPs mass ratios and vice versa. The dispersion lead to dissolution of zinc oxide nanoparticles in water systems are highly dependent to the systems conditions (such as ionic strength (IS) and pH) (Domingos et al., 2013). Similar outcomes have been cited (Bian et al., 2011; Majedi et al., 2014; Peng et al., 2017) and documented that zinc oxide NPs aggregation highly depends on the adsorption of natural organic matters, IS and pH of the aqueous media (Ahamed et al., 2021).

However, natural waters or domestic and commercial wastewaters contain many manufactured contaminants which is caused by the direct or indirect influence of human activities (Wilkinson et al., 2017). The task for the determination of risks linked with the discharge of nanoparticles is ambiguity concerning the properties of nanoparticles that are altered once they interact with the environmental matrices (Handy and Shaw, 2007). The behaviour of ZnO-NPs could be altered by the presence of organic contaminants. For example, the surface charge values of ENPs (ZnO and TiO_2) were enhanced in magnitude in simulated waters with the addition of polybrominated diphenyl ethers (PBDEs), and the presence of PBDEs exhibited a strong influence on the hydrodynamic diameter, zeta potential (surface charge values), and aggregation of NPs (Khan et al., 2019; Wang et al., 2018). Thus, there is a need to investigate the chemistry of zinc oxide NPs in the existence of organic pollutants under environmental relevant circumstances, such as in the existence of organic matter, contaminants, and salts.

Among numerous persistent organic pollutants, brominated flame retardants (BFRs) are used globally due to their minimal influence on the properties of commercial products and cost-effectiveness comparing to other flame retardants (Waaijers and Parsons, 2016). However, more than 75 BFRs are recognised as persistent, bioaccumulative, and toxic to living entities (Kodavanti and Loganathan, 2019). The majority of BFRs can certainly leach into environment during their usage, discard, or reprocessing of consumer products. BFRs are frequently detected in sludge and sediment samples from wastewater treatment plants throughout the world due to their wide application, where they can interact with other co-existing ENPs (e.g ZnO, TiO_2 etc.) to form more or less complex compounds (De Wit, 2002; Demirtepe and Imamoglu, 2019; Kodavanti and Loganathan, 2019). HBCD is worldwide extensively employed BFR after polybrominated diphenyl ethers (PBDEs) and tetrabromobisphenol-A (Marvin et al., 2011). HBCD, an additive brominated flame retardant, is a very lipophilic ($\log K_{ow} = 5.6$) and persistent material (3 days half-life in air and 2025 days in water) (Kodavanti et al., 2017, 2011). It is commonly employed in cushioning textiles, expanded polystyrene foams, electrical gear and extruded polystyrene foam for thermal insulation in buildings (Cao et al., 2018). Global production of HBCD containing materials has expanded from 16,700 tons to 31,000 tons from 2001 to 2011 (Cao et al., 2018). The HBCD can be released into the environment through emission and releasing during production and consumption of products (e.g. polystyrene foam, paint, carpets, plastics, children's toys, craft materials, insulation and decorative polystyrene) (Covaci et al., 2006; Okonski et al., 2018). Different releasing processes lead to the presence of HBCD in air, biota, sediment and water (Cao et al., 2018;

Lara et al., 2018), in blood (Fromme et al., 2016) and breastmilk (Lu et al., 2018). HBCD has been registered in Annex A of the Stockholm Convention on POP (persistent organic pollutants) in 2013 because of its environmental persistence nature, bioaccumulation and toxicity (Jiang et al., 2020).

In this study, HBCD was used as a representative organic pollutant to investigate its interaction with ZnO-NPs in simulated waters and whether this interaction influence the fate of zinc oxide NPs. In particular, the dissolution of these nanoparticles in MilliQ water at various pH values was observed. The physicochemical properties and colloidal stability before and after interacting with HBCD in various simulated water conditions were investigated, such as in the existence of different salt concentrations and HA as dissolved organic matter.

2. Materials/chemicals and methods

2.1. Materials/chemicals

Hexabromocyclododecane powder (95%), zinc oxide nanoparticles, HA, NaCl, $MgCl_2$, $CaCl_2$ and acetone were acquired from (Sigma-Alrdich), Australia. All materials/chemicals were utilised as received.

2.2. Characterisation methods

Samples morphology were inspected by employing field emission scanning electron microscopy (FE-SEM) at an electron voltage of 15 kV after sputter coating the samples with a 10 nm platinum layer. Microstructures were studied using transmission electron microscopy (TEM) and was performed at 200 kV. Brunauer–Emmett–Teller (BET) and BJH sorption/desorption curve estimated at a relative pressure (P/P_o) of 0.30 and 0.99 were used for calculation of specific surface area and total pore volume (V_t). Non-local density functional theory (NLDFT) was used to measure the pore size distribution from the N_2 adsorption branch using micromeritics TriStar II. The micropore volume (V_{micro}) was calculated from t-plot method (Table S1).

Fourier transform infrared spectroscopy (FTIR) was used to know the functional groups before and after interactions. An X-ray powder diffraction (XRD) (Empyrean Malvern Panalytical) was employed to study the phase dimensional identification of nanoparticles, HBCD powder and HA. Thermogravimetric analysis (TGA) was employed to check the thermal response and stability of materials. Inductively coupled plasma mass spectrometry (ICP-MS), PerkinElmer's NexION 350x was used to determine the concentrations (mg/L) of dissolved zinc (Zn). Surface charge and particle size analysis using a Malvern Panalytical Zetasizer were performed to identify the surface charge values and agglomeration of zinc oxide NPs alone and with the existence of HBCD, HA and different electrolytes in pure water condition (MilliQ water).

2.3. Interactions between ZnO-NPs, HBCD and HA

The ZnO-NPs stock suspension was prepared by taking 0.1 gram of ZnO-NPs into 1 litre MilliQ water, followed by sonicating the system for 10 min. Numerous compositions of HBCD (0, 1, 2, 3, 4 and 5 mg/L) in MilliQ waters, containing the ZnO-NPs (0.1 g/L) suspension were prepared. The influence of salt (NaCl) on the interactions of ZnO-NPs with HBCD were also investigated. The effect of HA on the size and surface of zinc oxide NPs was investigated with and without the existence of HBCD (5 mg/L) and various electrolytes (NaCl, $CaCl_2$ and $MgCl_2$). To dissolve HA, 0.1 M sodium hydroxide (NaOH) solution was used. Many compositions of HA (0, 1, 2, 3, 4 and 5 mg/L) in the ZnO-NPs (0.1 g/L) suspension were prepared. The prepared suspensions were well mixed and homogenised for 24 h on orbital shaker at 150 revolution/min and then the suspensions were placed in a stationary position for the remainder of the 1-week or 3-weeks period. The pH of all the samples (range: 6.5–7.7) was maintained at 7.00 ± 0.02 by using 0.1 M hydrochloric acid (HCl) and 0.1 M sodium hydroxide (NaOH) buffer solution, followed by agitation for 1 h prior to analysis. Zetasizer (Malvern Pananalytical) was employed to calculate the charge values on the surface of ZnO-NPs using disposable folded capillary cells at room temperature.

After zeta potential experiments, 10 mL of 5 mg/L HBCD was centrifuged at 14,000 revolution/min for 45 min. The settled down nanoparticles were obtained and rinsed with MilliQ water prior to being centrifuged again to collect the nanoparticles for further analysis. The collected nanoparticles were air dried prior to further morphological and compositional analysis.

3. Results and discussion

3.1. Characterisation of ZnO-NPs, HBCD and HA

3.1.1. Surface morphology analysis

The morphology of ZnO-NPs was examined using FE-SEM and TEM (Fig. 1). The ZnO-NPs are aggregated spongy particles (Fig. 1a). Majority of the particles are $\leq$100 nm, but some particles were found to be larger than Sigma-Aldrich supplied reading ($<$ 100 nm particle size) (Fig. 1, b and d). ZnO-NPs are either rod or spherical shaped (Gupta et al., 2006;

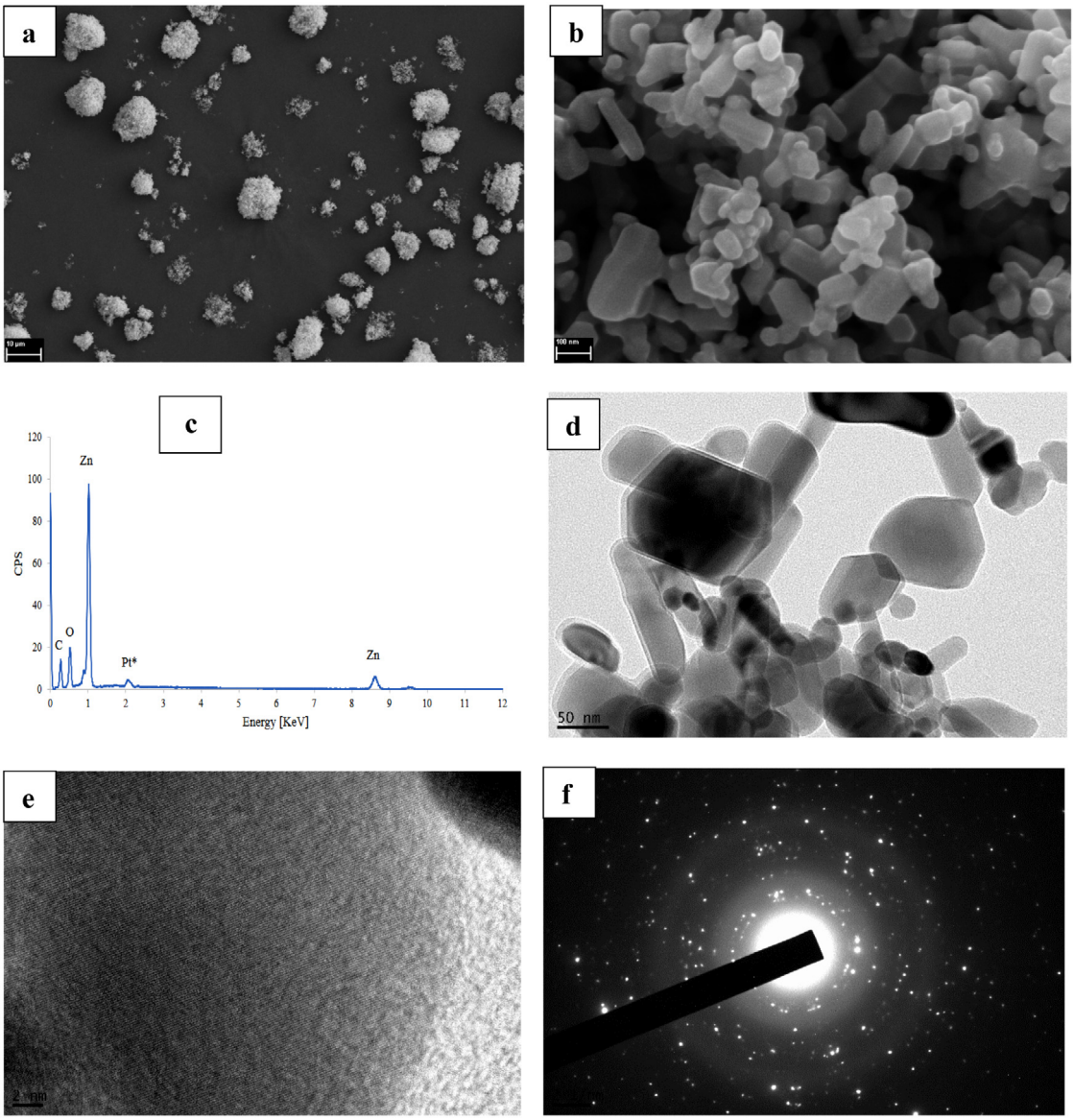

Fig. 1. Morphology and element analysis of ZnO-NPs by FE-SEM (a, b), elemental composition analysis (c) and TEM (d, e, f).

Lin et al., 2014). Elemental composition analysis (Fig. 1c) of purchased zinc oxide nanoparticles indicates the existence of both zinc and oxygen. TEM image (Fig. 1d) further confirmed the morphology of ZnO-NPs, indicating both spheres and rod-like shapes and a particle size of $\leq$100 nm. The ordered structure of ZnO-NPs observed at 2-nm is shown in Fig. 1e. The presence of bright spots or rings (Fig. 1f) indicate the preferential orientation of nanocrystals or crystalline/ordered structure of ZnO-NPs (Gupta et al., 2006; Khoshhesab et al., 2011; Talam et al., 2012; Zak et al., 2011).

3.1.2. Pore size analysis

The BET/BJH analysis of zinc oxide NPs is exhibited in Fig. S1. The nitrogen adsorption/desorption isotherm (Fig. S1a) of ZnO-NPs shows an isotherm (category IV) with hysteresis loop (H_3), indicating the mesoporous surface of nanoparticles having slit resembling pores (Pudukudy and Yaakob, 2015; Senapati et al., 2012). The SSA (specific surface area) calculated by the BET and Langmuir methods are 11.26 m^2/g and 27.51 m^2/g respectively (Table S1). The BJH graph was employed to calculate the pore size distribution of NPs (Fig. S1b). ZnO-NPs samples determined by NLDFT with a slit shape pore model exhibit a bimodal pore size distribution mostly in mesopores (2–15 nm) region, demonstrating a sufficient mesoporosity structure (Liu et al., 2015).

3.1.3. Mineralogical analysis

The mineralogical analysis of ZnO-NPs was determined using XRD and was shown in Fig. 2a. Sharp peaks at 2θ values of 31.71°, 34.43° and 36.79° for ZnO-NPs indicating hexagonal wurtzite crystal structure with three utmost favoured alignments (1 0 0), (0 0 2) and (1 0 1), also agreeing with joint committee on powder diffraction standards (JCPDS, N0-36-1451) (Zak et al., 2011).

The functional groups of zinc oxide NPs, HA and HBCD are exhibited in FTIR (Fig. 2b). Peak at 430 cm^{-1} was because of the vibration of Zn–O that is the normal range (400–600 cm^{-1}) for metal oxides (Chandrasekar et al., 2020; Gharagozlou and Naghibi, 2016) for ZnO-NPs. The peaks at 2800–3000 cm^{-1} followed by 1400–1470 cm^{-1} confirm the oscillation of (CH_2) and (C–H) within the molecule of organic pollutant (HBCD). The peaks at 600–1300 cm^{-1} represent alicyclic vibration (C–C), which could be due to the alicyclic skeleton of organic pollutant (HBCD). The peaks at 500–700 cm^{-1} represent stretching vibration which could be due to (C–Br) in the organic pollutant (HBCD) (Zhang et al., 2014). HA showed absorbance peaks at 2987 cm^{-1} and 1500 cm^{-1} attributing to aliphatic C–H asymmetric stretching vibration and the presence of some metallic cations (Sudiono et al., 2017). The peaks at 1145 and 840 cm^{-1} may be because of C–O stretching and C–H bending (Stuart, 2004).

TGA and differential thermogravimetric analysis (DTG) thermographs of HBCD and HA powders were analysed under nitrogen condition, which are shown in Fig. S2 (a,b). HBCD starts degrading at ∼225 °C with significant weight loss (89 ± 1%) occurred at 235 °C to 290 °C. Around 6 ± 1% residual mass are recognised as carbon ash (Faridvand et al., 2016). However, HA shows several steps of weight loss, around 367 °C and 473 °C. Dehydration occurred till 200 °C and then removal of functional groups (from 250 °C to 300 °C), and lastly breakdown of nuclei beyond 400 °C. Residual mass 32 ± 1% at a very high temperature of 896 °C could be attributed to the presence of highly thermally stable metallic complexes (Santos et al., 2018).

3.1.4. Impact of pH on the dissolution of zinc oxide nanoparticles

ZnO-NPs exhibit a very low dissolution nearly at neutral pH. The dissolution rate is directly proportional to the particles surface area. The dissolution of NPs would be rapid compared to the materials in bulk. This is represented in the following Noyes–Whitney's equation (Bian et al., 2011).

$$\frac{dm}{dt} = \frac{DA}{h}(c_s - c) \tag{1}$$

Where, dm/dt represents dissolution rate, A denotes surface area, D denotes diffusion coefficient, h denotes the diffusion layers' thickness, c_s and c represent the saturation and bulk concentrations respectively.

Moreover, the particles solubility depend on their size, smaller the particle size, higher the solubility, indicated from thermodynamically and improved form of the Kelvin equation, which could be explained according to the subsequent Ostwald–Freundlich equation (Bian et al., 2011).

$$\frac{S}{S_0} = \exp\left(\frac{2\gamma V_m}{RTr}\right) \tag{2}$$

Where, S represents particles solubility and (r) their radius in metre, S_0 denotes bulk materials solubility, V_m denotes molar volume and γ, R and T represent the surface free energy, gas constant and temperature respectively.

In this study, ZnO-NPs (0.1 g/L) were used for investigation which showed the majority of the particles are ≤100 nm with some particles/aggregates larger than Sigma-Aldrich supplied reading (<100 nm particle size), Fig. 1 (b and d). The average concentration (mg/L) of dissolved zinc in the MilliQ water at varying pH is presented in Fig. 2c. The understanding of dissolution of zinc oxide nanoparticles is essential to investigate their toxicity and stability behaviour in aqueous media (Bian et al., 2011).

In the ZnO-NPs suspension (0.1 g/L), ZnO surface could be hydrolysed to form a layer of hydroxide and zinc hydroxide, $Zn(OH)_2$ is moderately water soluble (Bian et al., 2011). Fig. 2c depicts that at highly acidic conditions such as pH 2, 4 and 6 the concentration of dissolved zinc is high such as 42.6, 42.1, and 41.3 mg/L respectively. This shows that nanoparticles dissolution in MilliQ water is due to the attack of protons on the surface of nanoparticles. The soluble ionic forms of dissolved ZnO-NPs could include $Zn^{2+}_{(aq)}$ and $Zn(OH)^{+}_{(aq)}$ at pH ≤ 6 (Bian et al., 2011; Domingos et al., 2013; Yamabi and Imai, 2002). It can be seen that at pH 7 and 8, 10 and 12, much less dissolution of zinc has been observed with 1.3, 1.1, 0.5 and 0.4 mg/L respectively. In aqueous media (pH ≥ 9), the ZnO-NPs dissolution is directly associated with their hydroxide to generate soluble compounds in terms of some hydroxide compounds such as $Zn(OH)_{2(aq)}$, then $Zn(OH)^{-}_{3(aq)}$ and $Zn(OH)^{2-}_{4(aq)}$. The precipitates of $Zn(OH)_{2(s)}$ could present between pH 6 and 9 indicating the lowest solubility of ZnO-NPs in this pH range (Bian et al., 2011; Yamabi and Imai, 2002).

The results (Fig. 2c) indicated minimum release of $Zn^{2+}_{(aq)}$ and $Zn(OH)^{+}_{(aq)}$ at pH 7. Similarly, the formation of hydroxide complexes (e.g. $Zn(OH)^{2-}_{4(aq)}$, $Zn(OH)_{2(aq)}$ and $Zn(OH)^{-}_{3(aq)}$) is limited at pH 7 as compared to those generated at pH greater than 7. Based on these findings, the interactions between ZnO-NPs with HBCD with and without the presence of HA and electrolytes were investigated at pH 7. This study is conducted at pH 7.00 ± 0.02 where the dissolution of ZnO-NPs to form zinc ions and its soluble ions and hydroxides is prevented. The results presented in next sections are at pH 7.00 ± 0.02.

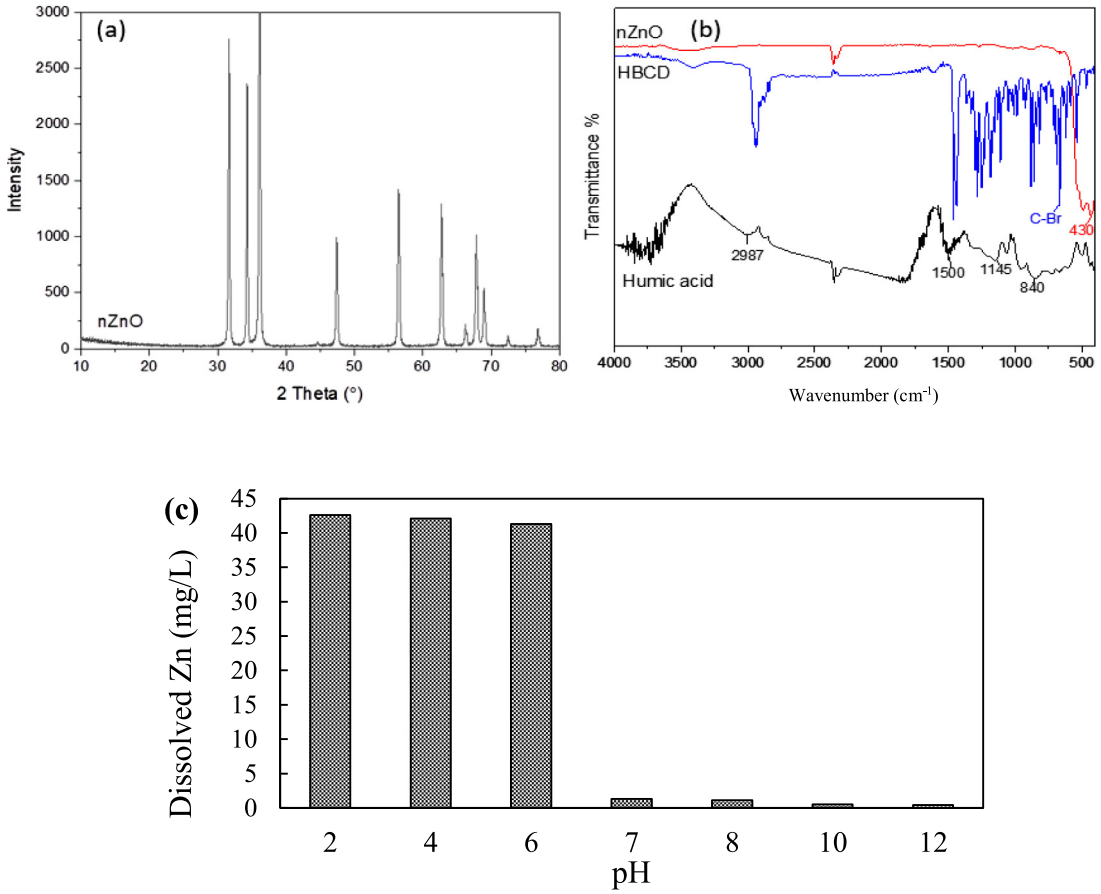

Fig. 2. XRD of ZnO-NPs (a), FTIR of ZnO-NPs, HBCD and HA (b), and concentration (mg/L) of dissolved Zn in milliQ water (c).

3.2. Influence and impact of HBCD on the size and zeta potential of ZnO nanoparticles

The size and zeta potential of zinc oxide NPs can be affected by the presence of HBCD, which was investigated under conditions with and without electrolytes (NaCl).

3.2.1. Influence/impact of HBCD on the hydrodynamic size of zinc oxide nanoparticles

The hydrodynamic size of nanoparticles in the existence of various concentrations of HBCD with and without monovalent (NaCl) electrolyte were analysed and shown in Fig. 3 (particle size at the peak of particle size distribution curve and shortly represented as "particle size (*d*, nm)") and Fig. S3 (particle size distribution (*d*, nm)). ZnO-NPs with particle size diameter 122 nm, are in the range of 68.1–400 nm in MilliQ water after 1 week of solution preparation. The presence of 1, 2, 3, 4 and 5 mg/L HBCD shifted the size of ZnO-NPs from 68.1 to 78.8, 78.8, 91.3, 106 and 106 nm respectively (Fig. S3a). The area under the curve also increased as the concentration of HBCD enhanced (Jasper et al., 2010). These findings show that PSD of zinc oxide nanoparticles are largely dependent on agglomeration, and their surface adsorption by organic pollutants (Khan et al., 2019; Kroll et al., 2014; Philippe and Schaumann, 2014; Wang et al., 2018). It can be seen that the nanoparticles size enhanced to some extent in existence of HBCD, which could be due to higher molecular weight of HBCD and surface coating on the ZnO-NPs because of hydrophobic and van der Waals interactions. Moreover, the increased PSD of nanoparticles in existence of HBCD associated to nanoparticles in pure MilliQ water indicates the less stable nature of nanoparticles in suspension and tend to aggregate in the presence of HBCD (Khan et al., 2019). Similar trends were obtained after placing the same solution in a stationary position for 3 weeks from the day of preparation (with shaking for the first 24 h only). The ZnO-NPs size distribution (Fig. S3b) in MilliQ water exhibited that the NPs are in the range of 68.1 – 955 nm, however, the presence of 1, 2, 3, 4 and 5 mg/L HBCD shifted the ZnO particle size from 68.1 to 106, 164, 190, 220 and 342 nm respectively. The area under the curve also increased as the concentration of HBCD elevated (Jasper et al., 2010).

To quantitatively evaluate the stabilising effects of HBCD on nanoparticles in aqueous systems, agglomeration kinetics of nanoparticles in existence of HBCD (5 mg/L), 100 mM and 200 mM NaCl were studied after 1 week and 3 weeks (Fig. 3

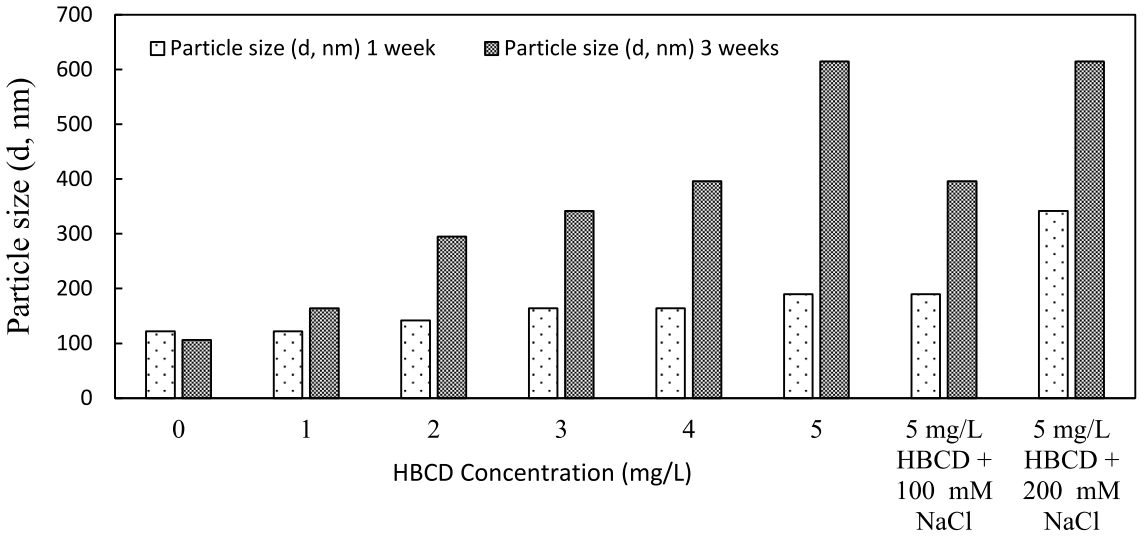

Fig. 3. ZnO-NPs size enlargement with various concentrations of HBCD with and without presence of NaCl as electrolyte.

and Fig. S3c). The agglomeration of ZnO-NPs increased with the addition of 100 mM and 200 mM NaCl. For instance, the particle size for ZnO-NPs with 5 mg/L HBCD ranged from 106 to 459 nm with particles size for most particles by number (%) as 190 nm, while the size range increased to 106–955 nm and 220–712 nm with maximum size of 190 nm and 342 nm (Fig. 3 and Fig. S3c) in the existence of 100 mM and 200 mM NaCl respectively. The same agglomeration increment trends were observed after 3 weeks. The particle size ranges were 225–825 nm and 342–955 nm with particles size for most particles by number (%) as 396 nm and 615 nm (Fig. 3 and Fig. S3c) in the existence of 100 mM and 200 mM NaCl respectively. The stability of nanoparticles in the presence of salt depends heavily on the capping agents used for the stabilisation of nanoparticles (Zhang et al., 2012). HBCD-capped ZnO-NPs are negatively charged (as shown in Fig. 4) and stable, which means HBCD as a capping agent, can direct interact with the surface OH groups of ZnO-NPs. The interactions are rather hydrophobic, indicating that HBCD accumulates at the particle surface was due to its poor interactions with water. On the other hand, the aggregation occurred in the presence of salt (e.g., 100 mM and 200 mM NaCl) could be due to charge screening and cations bridging effects. The ZnO-NPs approaching each other experience electrostatic and London attractive forces (Enustun and Turkevich, 1963; Zhang et al., 2012).

3.2.2. Influence of HBCD on the zeta potential of zinc oxide nanoparticles

Surface charge of ZnO nanoparticles (0.1 g/L nanoparticle dispersion) at pH 7.00 ± 0.02 adjusted by adding 1 mL pH 7.00 buffer solution (Horiba) was −43.9 mV (Fig. 4). The charge on the surface of nanoparticles became less negative with increasing concentrations of HBCD (Fig. 4). For example, the surface charge of ZnO-NPs altered from −43.9 mV (MilliQ water) to −38.4 mV in the existence of HBCD (5 mg/L). The alteration in the zeta potential values of ZnO-NPs with higher amounts of HBCD as an organic pollutant predicts that HBCD, similar to numerous other organic substances (Adeleye and Keller, 2016; Domingos et al., 2009; Wang et al., 2018; Xiao and Chen, 2016; Yu et al., 2018), can also adsorb on the surface of nanoparticles. The zinc oxide nanoparticles stability decreases with a rise in surface charge in the presence of HBCD, which can result in particles aggregation as proved by particle size distribution (Fig. S3a,b). A sharp alteration (high surface charge magnitude) of ZnO-NPs with and without HBCD was observed after stationary equilibrium for 3 weeks. The surface charge of ZnO-NPs altered from −43.9 mV (after 1 week) to −3.66 mV (after 3 weeks), and a same pattern was noticed with the existence of HBCD. For instance, the zeta potential for 1, 2, 3, 4 and 5 mg/L HBCD changed from −41.9, −41.7, −40.6, −39.1 and −38.4 mV (after 1 week) to −2.65, −2.38, −2.19, −1.39 and −0.105 mV (after 3 weeks), respectively. The presence of electrons (negative surface charge which may be attributed to deprotonated OH-groups at the ZnO surface) at the surface of ZnO-NPs particles became more significant with reducing of particle size (Cheng, 2006). It will also induce hydroxide (OH^-) in water systems to provide negative surface charges of nanoparticles (Cheng, 2006). The negative surface charge gradually decreased with the addition of various concentrations of HBCD which could be due to the coating effects of organic pollutant (HBCD) on the negatively charged surface of nanoparticles.

The presence of electrolytes (100 mM and 200 mM NaCl) further altered the charge on the surface of nanoparticles in existence of HBCD (5 mg/L) (Fig. 4). For instance, the zeta potential changed to −41.1 and −20.3 mV after 1 week, and to −0.66 to −0.32 mV after 3 weeks in the existence of 100 to 200 mM monovalent salt (NaCl). Such trends could be attributed to gathering of charged ions (positive) all over electric double layer surrounded by nanoparticles, screening of nanoparticles surface charge and making them less stable, which lead to agglomeration via electrostatic and London attraction (Enustun and Turkevich, 1963; MacCuspie, 2011).

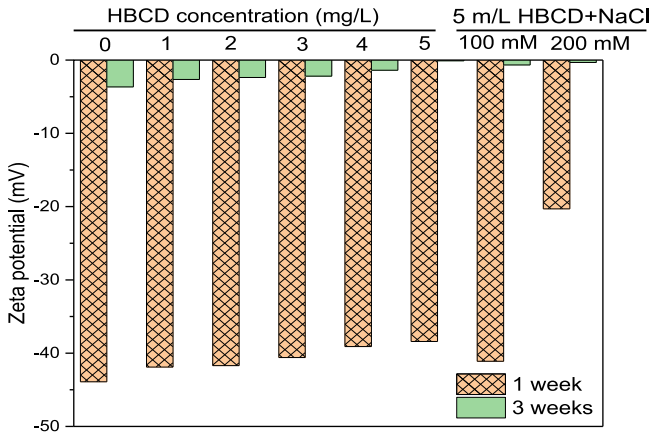

Fig. 4. Zeta potential of ZnO-NPs with HBCD and NaCl after stationary equilibrium for 1 and 3 weeks.

3.2.3. Investigation of ZnO-NPs and HBCD interactions by spectroscopy technique

ZnO nanoparticles and HBCD interactions were also investigated using UV (spectroscopy) technique. The absorption peak for the ZnO nanoparticles suspension in water appears at 376 nm indicating the hexagonal wurtzite ZnO-NPs (Pudukudy and Yaakob, 2015).

More absorbance of UV light was observed with increasing the concentration (Ahmad et al., 2013) of HBCD (Fig. S4a). For instance, the absorbance of UV-light was 0.067 at the peak height for pure ZnO-NPs suspension, and it increased from 1 to 5 mg/L of HBCD. Maximum absorbance was measured at the 5 mg/L HBCD peak i.e 0.201. It could be assumed that the ZnO-NPs strongly interact with HBCD molecules via van der Waals and hydrophobic interactions. Fig. S4b reveals the same trend of absorbance in the existence of electrolytes with various concentrations. It can be seen that the absorbance intensity increased from 0.067 (ZnO-NPs suspension) to 0.072 and 0.084 in the presence of 100 mM and 200 mM NaCl, respectively. These results can be linked with the increment in particle size and electrokinetic potential of zinc oxide NPs resulting in more stable internal interactions between the nanoparticles and the organic pollutant (HBCD). Nanoparticles are usually stabilised due to the adsorption of a layer of dispersed organic pollutant and/or dispersant layer (adlayer) covering the particle surface. However, the stabilisation of nanoparticles in a suspension highly depends on the formation of the adlayer of appropriate thickness. Excessive excluded volume could be expected around the surface of nanoparticles due to the formation of thick adlayers. On the other hand, thin adlayers also support the particles agglomeration (Studart et al., 2007).

3.2.4. Morphology and FTIR of ZnO-NPs after interactions with HBCD

The morphology and structure of zinc oxide nanoparticles and HBCD after 3 weeks of interaction (5 mg/L HBCD) were analysed using FE-SEM, EDS and FTIR which are shown in Fig. 5. Agglomeration/coagulation effects were observed in Fig. 5a–b, confirming the increase in particle size (ranging from $\leq$10 μm to $\geq$100 μm) after the interactions. Elemental composition analysis and mapping (Fig. 5c–e) revealed the presence of both zinc and bromine atoms after the interactions. The FTIR spectrum of ZnO-NPs after the interaction with HBCD was analysed (Fig. 5f). Absorbance at 671 cm^{-1} represents of stretching oscillation of (C–Br) tie which could be linked with adsorption of HBCD molecules onto the ZnO-NPs (Zhang et al., 2014). A small peak at 509 cm^{-1} could be attributed to the existence of ZnO-NPs which is in-between the normal metal oxide range (400–600 cm^{-1}) (Chandrasekar et al., 2020; Gharagozlou and Naghibi, 2016). After interaction, the FTIR of ZnO-NPs after interaction with HBCD (ZnO-NPs+HBCD) shows the presence of ZnO-NPs and HBCD as well. For instance, an absorbance peak at 543 cm^{-1} (Fig. 5f) indicate existence of metal oxide NPs (such as zinc oxide NPs). The peak at 671 cm^{-1} and peaks in the range of 600–1300 cm^{-1} and 2800–3000 cm^{-1} (Fig. 5f) support the presence of stretching vibration of (C–Br), alicyclic (C–C) vibration of the HBCD alicyclic skeleton and vibration of (C–H) chain in HBCD molecules respectively (Zhang et al., 2014).

3.3. Influence and impact of HA on the size and zeta potential of zinc oxide NPs

3.3.1. Influence/impact of HA on the size of zinc oxide NPs

Size distribution of ZnO nanoparticles in existence of various concentrations of HA with and without monovalent and divalent electrolytes is shown in Fig. 6 and Fig. S5. After 1 week of interactions (Fig. 6 and Fig. S5a) in MilliQ water, it is observed that the nanoparticles are typically in the range of 106–1720 nm with particle size (particle size at the peak of particle size distribution curve and shortly represented as "particle size (d, nm)") of 190 nm, while the ZnO-NPs size shifted to the range of 615–2670 nm in presence of 5 mg/L HA with maximum particle size of 1110 nm. The area under the curve also increased as the increase in concentration of HA, which may be because of coating/capping effects

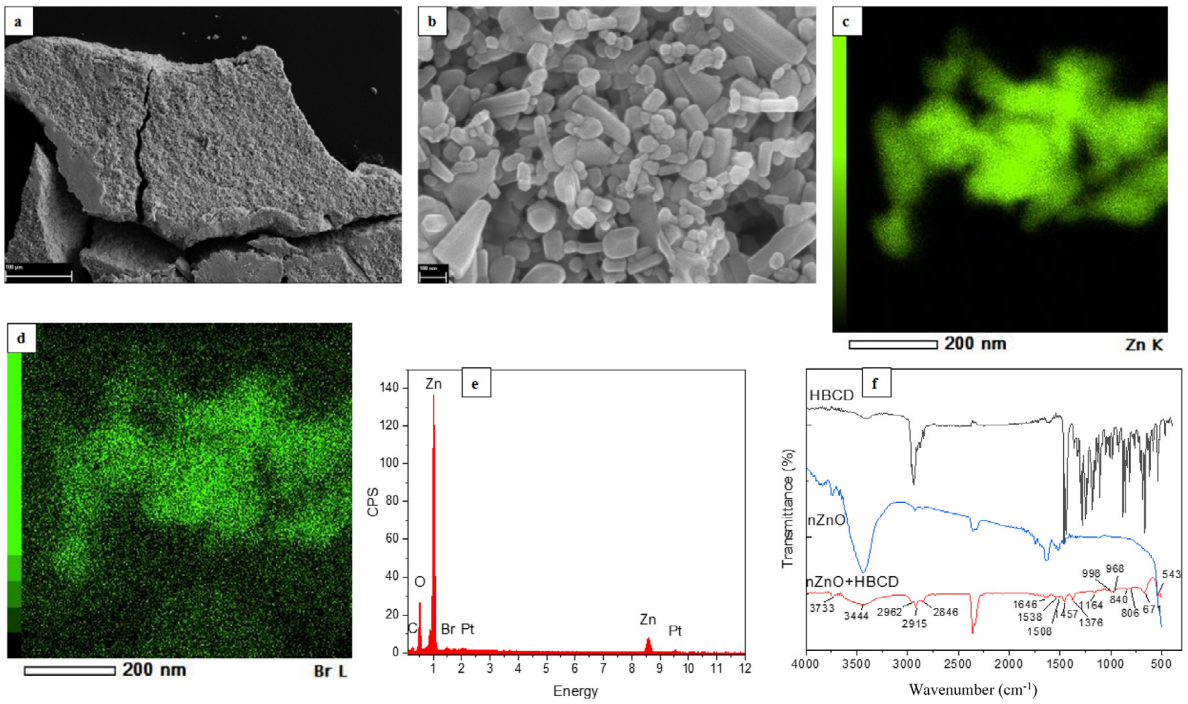

Fig. 5. SEM images (a, b), EDS (c, d, e), FTIR of the extracted sample, after 3 weeks of ZnO-NPs interactions with 5 mg/L HBCD (f).

of HA on nanoparticles' surface. Similar trends with less accumulative size compared with 1 week were observed for the size distribution of suspensions after 3 weeks of stationarity (Fig. 6 and Fig. S5b). The size ranges of ZnO-NPs and ZnO-NPs with 1, 2, 3, 4 and 5 mg/L HA were 122–615, 190–459, 220–1720, 255–712, 220–1720 and 459–1720 nm (Fig. S5b) with particle size of 190, 255, 342, 396, 712 and 825 nm (Fig. 6a), respectively. Similarly Baalousha (Baalousha, 2008) documented that HA adsorption onto the (iron oxide) NPs' surface also increased surface charge of the nanoparticles and their stability as well. Thio et al. (2011) documented that titanium dioxide nanoparticles were aggregated in water media, but significantly stabilised in the existence of HA. We could also assume that the breakup of aggregate occurs with time if the applied hydrodynamic splitting force on the aggregates is more compared to their (aggregates) on strength (Tambo and Hozumi, 1979). Therefore, once the applied hydrodynamic splitting force (F_{hyd}) on HA cluster becomes more than cluster overall strength ($F_{aggregate-cluster}$), cluster breakup occurs (Hakim et al., 2019).

The accumulation kinetics of zinc oxide nanoparticles with HA (5 mg/L) were investigated in the existence of 100 mM and 200 mM electrolytes (NaCl, $CaCl_2$ and $MgCl_2$) after 1 and 3 weeks of stationary equilibrium. The particle size range changed to 531–2670 nm (particle size, 1110 nm) and 825–2300 nm (particle size, 1280 nm) in the existence of 100 mM and 200 mM NaCl comparing to 615–2670 nm for ZnO-NPs with only 5 mg/L HA (Fig. 6b and Fig. S5a, c). A similar trend of particle size for nanoparticles were observed in the existence of 100 mM and 200 mM $CaCl_2$ and similar concentrations of $MgCl_2$ with 5 mg/L HA. The size range changed to 295–1480 nm (particle size, 615 nm) and 531–2300 nm (particle size, 1110 nm) in the presence of 100 mM and 200 mM $CaCl_2$ respectively, and to 459–1990 nm (particle size, 955 nm) and 825–3090 nm (particle size, 1280 nm) for $MgCl_2$ respectively (Fig. 6b and Fig. S5c). The particle size of the same suspensions was analysed after 3 weeks of stationary equilibration by adjusting their pH using acid/base concentrations as mentioned in Section 2.3. The size ranges in the presence of 100 mM and 200 mM were 295–1280 nm (particle size, 531 nm) and 531–1110 nm (particle size, 825 nm) for NaCl, 531–1720 nm (particle size, 955 nm) and 615–1990 nm (particle size, 1110 nm) for $CaCl_2$ and 531–1480 nm (particle size, 825 nm) and 459–1720 nm (particle size, 825 nm) for $MgCl_2$ respectively (Fig. 6 and Fig. S5d).

The variation in the size range could be due to the aggregation of NPs to lower their surface energy, blocking of the pore throats (i.e size of the particles present in the fluid are comparable or bigger than the size of the pore constrictions) and loss of their parental characteristics. The presence of electrolytes (e.g. NaCl, $CaCl_2$, and $MgCl_2$) can drastically stimulate the rate of coagulation and flocculation due to high degree of coalescence and collusion of nanoparticles followed by cation bridging, hydration forces, different ionic strengths and pH of the systems (Hakim et al., 2019; Liu et al., 2020). Similar reasons could be assumed in the effects of interactions of HBCD, HA, monovalent and divalent electrolytes on the size distribution of ZnO-NPs are demonstrated (Fig. 6c and Fig. S5e-f). It can be seen (Fig. S5e) that size range of nanoparticles increased in the existence of HBCD, but the existence of HA with electrolytes further increased the particle size ranges of nanoparticles. Agglomeration (825–7460 nm with particle size, 1720 nm) of the nanoparticles due to the existence of both

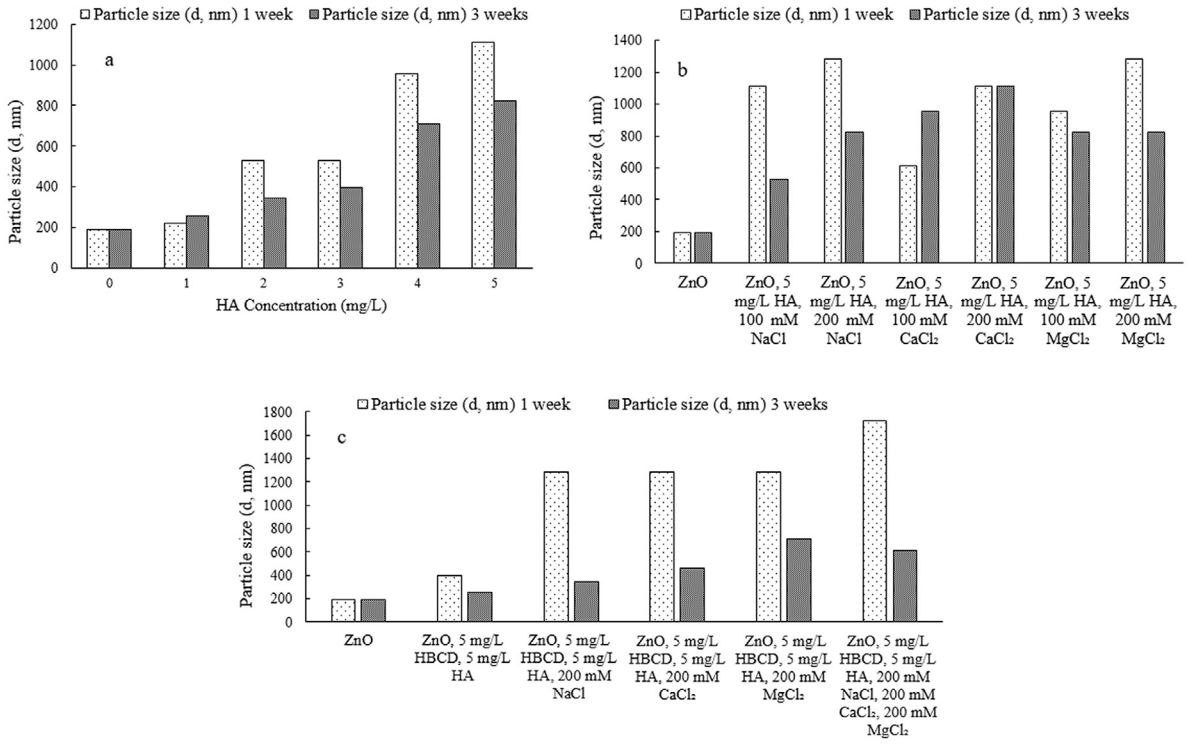

Fig. 6. ZnO-NPs size in the existence of HBCD, HA and electrolytes.

HBCD and HA (with fixed amount, 5 mg/L) and 200 mM of different electrolytes revealed that the fate and behaviour of ZnO-NPs could be altered after interacting with other organic/inorganic substances. Fig. S5f illustrates the same trends in particle size changes after 3 weeks' time. For instance, the range of the particle size was 825–7460 nm (after one week, Fig. S5e) which reduced to 220–3090 nm after 3 weeks, (Fig. S5f). This behaviour may be related to the existence of organic acid, particularly the HA, which influences the transport of ENPs such as ZnO-NPs by reducing the aggregation (Han et al., 2014; Jahan et al., 2017). Two constraints can impact on adsorption capability of organic contaminants by adsorbents: the integer of explicit affinity positions and affinity coefficient of explicit positions towards pollutants. Improved ENPs stability or segregation of generous ENPs agglomerates by adsorbed dissolved organic matters can raise the total count of explicit affinity positions, which supports the adsorption of organic pollutants. Concurrently, the adsorbed organic matters may also yield new affinity positions and/ or block the ENPs affinity positions to alter their adsorption capacity for organic pollutants. Dissolved organic matters, which are not adsorbed by the nanoparticles, may also comparatively adsorb the pollutants and hence cut off the further adsorption of pollutants on the ENPs surface (same as in our research outcomes) (Yu et al., 2018). A similar trend in the reduction of particle sizes after 3 weeks of interactions can be observed (Fig. 6c).

3.3.2. Influence of HA on the zeta potential of zinc oxide nanoparticles

The pH of ZnO nanoparticles (0.1 g/L nanoparticles dispersion) and other solutions prepared with HA was maintained using acid (0.1M hydrochloric acid, HCl) and base (0.1M sodium hydroxide, NaOH) solutions. Surface charge values of nanoparticles suspension increased in magnitude (became more negative) with addition of increasing concentrations of HA after 1-week of stationary. Surface charge values of nanoparticles increased from −5.8 mV in MilliQ water to −11.2, −11.7, −19.6, −19.6 and −19.5 mV in the existence of 1,2,3,4 and 5 mg/L HA respectively (Fig. 7). This suggested that HA can interact/coat the ZnO-NPs and can alter surface charge values of nanoparticles in suspension, which is same to the findings reported by (Mohd Omar et al., 2014). Agglomeration, segregation or stabilisation of nanoparticles (ZnO-NPs) is dependent on the environmental conditions such as pH, humic substances to NPs' concentration ratio and physico-chemical characteristics of the natural organic substances. However, the adsorption/coating of humic substances to the surface of particular nanoparticles can increase their surface charge (zeta potential) and stability in aqueous media (Baalousha, 2008; Mohd Omar et al., 2014).

Same pattern was noticed (Fig. 7) with the same suspensions after 3 weeks. For example, surface charge of nanoparticles (−7.45 mV) increased in magnitude to −11.1, −13.2, −14.2, −16.2 and −18.2 mV in the existence of 1, 2, 3, 4 and 5 mg/L HA respectively.

The presence of electrolytes (100 mM and 200 mM NaCl) further increased the surface charges of nanoparticles in the existence of HA (5 mg/L) (Fig. 7). This could be because of gathering of the ions all over electric double layer surrounded by

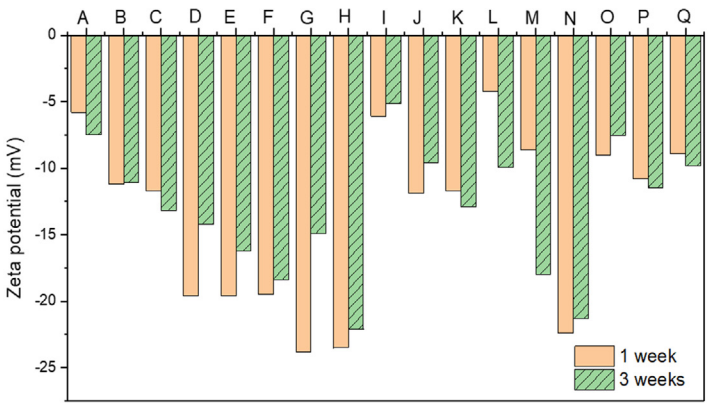

	nZnO (g/L)	HA (mg/L)	HBCD (mg/L)	NaCl (mM)	$CaCl_2$ (mM)	$MgCl_2$ (mM)
A	0.1	0				
B	0.1	1				
C	0.1	2				
D	0.1	3				
E	0.1	4				
F	0.1	5				
G	0.1	5		100		
H	0.1	5		200		
I	0.1	5			100	
J	0.1	5			200	
K	0.1	5				100
L	0.1	5				200
M	0.1	5	5			
N	0.1	5	5	200		
O	0.1	5	5		200	
P	0.1	5	5			200
Q	0.1	5	5	200	200	200

Fig. 7. Surface charge values of ZnO-NPs with HA, HBCD, monovalent and divalent electrolytes and their mixture after 1 and 3 weeks stationary time.

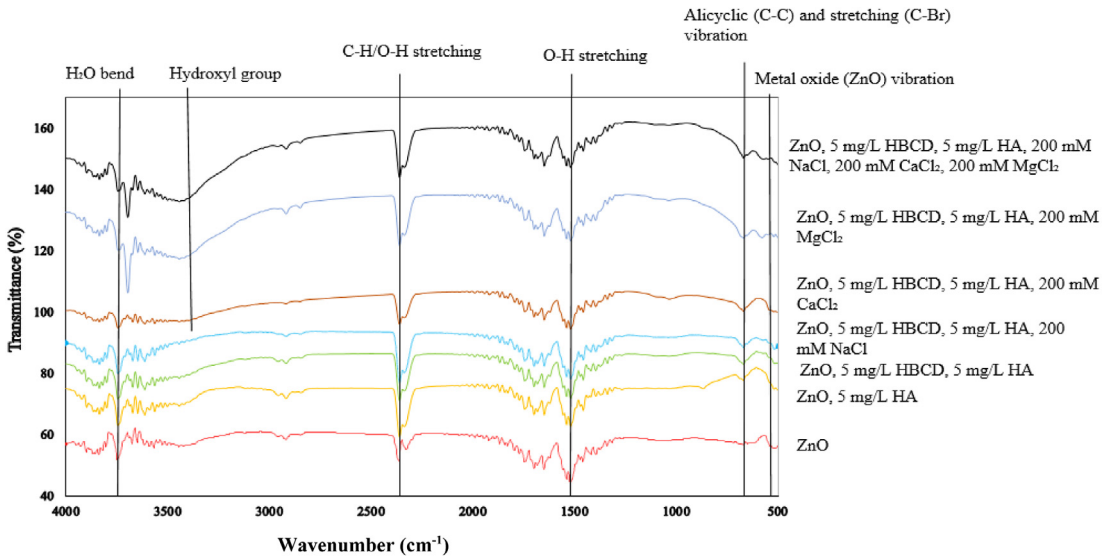

Fig. 8. FTIR of the extracted samples, after 3 weeks of ZnO-NPs interaction with 5 mg/L HBCD, 5 mg/L HA and 200 mM of various salts.

nanoparticles, shielding the NPs' surface charge and making them more unstable via electrostatic attraction. The presence of divalent cations (Ca^{2+}) 100 mM and 200 mM in the ZnO-NPs suspension with 5 mg/L HA increased the surface charge values with increase of divalent cations concentrations. For instance, the zeta potential values are, i.e −6.09 mV for 100 mM $CaCl_2$ to −11.9 mV for 200 mM $CaCl_2$ for samples after 1 week equilibration. Similar trend was observed for 3 weeks stationary time placement as well (Fig. 7). This could be attributed to the gathering of more ions all over the electric double layer of the nanoparticles. On the other hands, presence of divalent cations (Mg^{2+}) 100 mM and 200 mM in NPs suspension with HA (5 mg/L) exhibited different trends. For instance, zeta potential value for 100 mM $MgCl_2$ is −11.7 mV and decreased to −4.23 mV for 200 mM $MgCl_2$. This behaviour could be due to the ligand interactions of Mg^{2+} with HA (Hakim et al., 2019; Kawaguchi and Kyuma, 1959). The same trend in zeta potential was measured after 3 weeks of stationary time (Fig. 7). It can be seen that the surface charge values are in the range of -10 ± 2 mV (Fig. 7), except for 200 mM NaCl.

3.3.3. FTIR of ZnO-NPs after interactions with HBCD, HA and salts

Elemental composition analysis of pure salts (e.g, NaCl, $CaCl_2$ and $MgCl_2$) and the ZnO-NPs after interaction with organic pollutant (HBCD), HA and salts has been demonstrated in Fig. S6 and Fig. 8 respectively. In Fig. 8, the absorbance peaks at 528 cm^{-1}, 667 cm^{-1}, 1500 cm^{-1}, 2360 cm^{-1}, and 3745 cm^{-1} denote the presence of ZnO-NPs, Alicyclic (C–C) and stretching (C–Br) vibration, O-H stretching, C–H/O–H stretching and H_2O bend (Chandrasekar et al., 2020; Gharagozlou and Naghibi, 2016; Zhang et al., 2014) respectively which are the strong evidence of the presence of ZnO-NPs, HBCD and HA.

The presence of HBCD and HA influenced the surface charge, surface chemistry, particle size and morphology of ZnO-NPs. The alterations can occur for their agglomeration state, crystallinity morphology, purity, size, surface chemistry and toxicity. A summary of all analysis and conditions used in this study is tabulated in Table S2.

4. Conclusions

We investigated the particle size, surface charge and functional groups of zinc oxide nanoparticles before and after the interactions with HBCD under different conditions. The results showed increased particle size and enlarged surface charge density of zinc oxide nanoparticles, due to coating of the surface of nanoparticles with HBCD as a capping agent. The monovalent and divalent cations could alter nanoparticles' fate in the existence of HBCD. The natural organic matter (HA) can also influence on particle size. This study indicated that HBCD, HA and cations can alter the shape, size, surface chemistry and crystallinity of precursor zinc oxide nanoparticles in simulated waters. The results could provide indications for the fate and behaviour of zinc oxide nanoparticles after releasing into salty surface water or sea water.

CRediT authorship contribution statement

Anwar Ul Haq Khan: Conceptualization, Methodology, Investigation, Formal analysis, and Initial draft write-up. **Yanju Liu:** Supervision, Conceptualization, Writing – review & editing. **Ravi Naidu:** Supervision, Funding procurement, Writing – review & editing. **Cheng Fang:** Supervision, Writing – review & editing. **Raja Dharmarajan:** Supervision, Writing – review & editing. **Hokyong Shon:** Supervision, Writing – review & editing.

Declaration of competing interest

The authors declare that they have no known competing financial interests or personal relationships that could have appeared to influence the work reported in this paper.

Acknowledgements

The first author acknowledge, The University of Newcastle (UON), Australia, for granting the fully funded PhD (ECRHDR UNRS Central and UNIPRS) scholarship. The authors are grateful to CRC CARE and GCER, UON Callaghan, NSW 2308, Australia, for giving the financial assistance and research facilities to accomplish the presented task. Authors also acknowledge the support of Professor Graeme Jameson, Mrs. Kitty Tang, and Mr. Lonn Cooper from the Centre for Multiphase Processes, UON, for providing the facilities and training to conduct nanoparticles' size and surface analysis. Authors are grateful to Dr. Huiming Zhang and Dr. Yun Lin from the EMX (Electron Microscope and X-ray) unit, UON for providing the training and the SEM/TEM analysis facilities.

Appendix A. Supplementary data

Supplementary material related to this article can be found online at https://doi.org/10.1016/j.eti.2021.102078.

References

Adeleye, A.S., Keller, A.A., 2016. Interactions between algal extracellular polymeric substances and commercial TiO2 nanoparticles in aqueous media. Environ. Sci. Technol. 50, 12258–12265. http://dx.doi.org/10.1021/acs.est.6b03684.

Ahamed, A., Liang, L., Lee, M.Y., Bobacka, J., Lisak, G., 2021. Too small to matter? Physicochemical transformation and toxicity of engineered nTiO2, nSiO2, nZnO, carbon nanotubes, and nAg. J. Hazard. Mater. 404, 124107. http://dx.doi.org/10.1016/j.jhazmat.2020.124107.

Ahmad, M., Iqbal, Z., Hong, Z., Yang, J., Zhang, Y., Khalid, N.R., Ahmed, E., 2013. Enhanced sunlight photocatalytic performance of hafnium doped ZnO nanoparticles for methylene blue degradation. Integr. Ferroelectr. 145, 108–114. http://dx.doi.org/10.1080/10584587.2013.788943.

Ali, D., Alarifi, S., Kumar, S., Ahamed, M., Siddiqui, M.A., 2012. Oxidative stress and genotoxic effect of zinc oxide nanoparticles in freshwater snail Lymnaea luteola. L. Aquat. Toxicol. 124–125, 83–90. http://dx.doi.org/10.1016/j.aquatox.2012.07.012.

Baalousha, M., 2008. Aggregation and disaggregation of iron oxide nanoparticles : Influence of particle concentration, pH and natural organic matter. Sci. Total Environ. 407, 2093–2101. http://dx.doi.org/10.1016/j.scitotenv.2008.11.022.

Bian, S.W., Mudunkotuwa, I.A., Rupasinghe, T., Grassian, V.H., 2011. Aggregation and dissolution of 4 nm ZnO nanoparticles in aqueous environments: Influence of pH, ionic strength, size, and adsorption of humic acid. Langmuir 27, 6059–6068. http://dx.doi.org/10.1021/la200570n.

Bundschuh, M., Filser, J., Lüderwald, S., Mckee, M.S., Metreveli, G., Schaumann, G.E., Schulz, R., Wagner, S., 2018. Nanoparticles in the environment : where do we come from, where do we go to? Environ. Sci. Eur. 30, 1–17. http://dx.doi.org/10.1186/s12302-018-0132-6.

Caballero-Guzman, A., Nowack, B., 2016. A critical review of engineered nanomaterial release data: Are current data useful for material flow modeling? Environ. Pollut. 213, 502–517. http://dx.doi.org/10.1016/j.envpol.2016.02.028.

Cao, X., Lu, Y., Zhang, Y., Khan, K., Wang, C., Baninla, Y., 2018. An overview of hexabromocyclododecane (HBCDs) in environmental media with focus on their potential risk and management in China. Environ. Pollut. 236, 283–295. http://dx.doi.org/10.1016/j.envpol.2018.01.040.

Chandrasekar, M., Panimalar, S., Uthrakumar, R., Kumar, M., Saravanan, M.E.R., Gobi, G., Matheswaran, P., Inmozhi, C., Kaviyarasu, K., 2020. Preparation and characterization studies of pure and Li+ doped ZnO nanoparticles for optoelectronic applications. Mater. Today Proc. 2018–2021. http://dx.doi.org/10.1016/j.matpr.2020.03.228.

Cheng, K.L., 2006. The negative charge of nanoparticles. Microchem. J. 82, 119–120. http://dx.doi.org/10.1016/j.microc.2005.11.002.

Choi, S., Johnston, M., Wang, G.-S., Huang, C.P., 2018. A seasonal observation on the distribution of engineered nanoparticles in municipal wastewater treatment systems exemplified by TiO2 and ZnO. Sci. Total Environ. 625, 1321–1329. http://dx.doi.org/10.1016/j.scitotenv.2017.12.326.

Covaci, A., Gerecke, A.C., Law, R.J., Voorspoels, S., Kohler, M., Heeb, N.V., Leslie, H., Allchin, C.R., Boer, J.De., 2006. Hexabromocyclododecanes (HBCDs) in the environment and humans: A review. Environ. Sci. Technol. 40, 3679–3688. http://dx.doi.org/10.1021/es0602492.
De Wit, C.A., 2002. An overview of brominated flame retardants in the environment. Chemosphere 46, 583–624. http://dx.doi.org/10.1016/S0045-6535(01)00225-9.
Demirtepe, H., Imamoglu, I., 2019. Levels of polybrominated diphenyl ethers and hexabromocyclododecane in treatment plant sludge: Implications on sludge management. Chemosphere 221, 606–615. http://dx.doi.org/10.1016/j.chemosphere.2019.01.060.
Domingos, R.F., Rafiei, Z., Monteiro, C.E., Khan, M.A.K., Wilkinson, K.J., 2013. Agglomeration and dissolution of zinc oxide nanoparticles: role of pH, ionic strength and fulvic acid. Environ. Chem. 10, 306–312.
Domingos, R.F., Tufenkji, N., Wilkinson, K.J., 2009. Aggregation of titanium dioxide nanoparticles: Role of a fulvic acid. Environ. Sci. Technol. 43, 1282–1286. http://dx.doi.org/10.1021/es8023594.
Enustun, B., Turkevich, J., 1963. Coagulation of colloidal gold. J. Am. Chem. Soc. 85, 3317–3328. http://dx.doi.org/10.1021/ja00904a001.
Fahmy, S.R., Sayed, D.A., 2017. Toxicological perturbations of zinc oxide nanoparticles in the coelatura aegyptiaca mussel. Toxicol. Ind. Health 33, 564–575. http://dx.doi.org/10.1177/0748233716687927.
Falfushynska, H., Gnatyshyna, L., Yurchak, I., Sokolova, I., Stoliar, O., 2015. The effects of zinc nanooxide on cellular stress responses of the freshwater mussels unio tumidus are modulated by elevated temperature and organic pollutants. Aquat. Toxicol. 162, 82–93. http://dx.doi.org/10.1016/j.aquatox.2015.03.006.
Faridvand, R., Peighambardoust, S.J., Shenavar, A., 2016. Preparation of flame retardant polystyrene via in-situ bulk polymerization method and evaluation of its flammability properties. Iran. J. Chem. Eng. 13, 62–70.
Fromme, H., Hilger, B., Albrecht, M., Gries, W., Leng, G., Völkel, W., 2016. Occurrence of chlorinated and brominated dioxins/furans, PCBs, and brominated flame retardants in blood of German adults. Int. J. Hyg. Environ. Health 219, 380–388. http://dx.doi.org/10.1016/j.ijheh.2016.03.003.
Gagné, F., Auclair, J., Peyrot, C., Wilkinson, K.J., 2015. The influence of zinc chloride and zinc oxide nanoparticles on air-time survival in freshwater mussels. Comp. Biochem. Physiol. Part C Toxicol. Pharmacol. 172–173, 36–44. http://dx.doi.org/10.1016/j.cbpc.2015.04.005.
Gagné, F., Auclair, J., Turcotte, P., Gagnon, C., Peyrot, C., Wilkinson, K., 2019. The influence of surface waters on the bioavailability and toxicity of zinc oxide nanoparticles in freshwater mussels. Comp. Biochem. Physiol. Part C Toxicol. Pharmacol. 219, 1–11. http://dx.doi.org/10.1016/j.cbpc.2019.01.005.
Gharagozlou, M., Naghibi, S., 2016. Sensitization of ZnO nanoparticle by vitamin B12: Investigation of microstructure, FTIR and optical properties. Mater. Res. Bull. 84, 71–78. http://dx.doi.org/10.1016/j.materresbull.2016.07.029.
Ghosh, M., Sinha, S., Jothiramajayam, M., Jana, A., Nag, A., Mukherjee, A., 2016. Cyto-genotoxicity and oxidative stress induced by zinc oxide nanoparticle in human lymphocyte cells in vitro and Swiss albino male mice in vivo. Food Chem. Toxicol. 97, 286–296. http://dx.doi.org/10.1016/j.fct.2016.09.025.
Gupta, A., Bhatti, H.S., Kumar, D., Verma, N.K., Tandon, R.P., 2006. Nano and bulk crystals of ZnO: Synthesis and characterization. J. Nanomater. Biostructures 1, 1–9.
Hakim, A., Suzuki, T., Kobayashi, M., 2019. Strength of humic acid aggregates: effects of divalent cations and solution pH. ACS Omega 4, 8559–8567. http://dx.doi.org/10.1021/acsomega.9b00124.
Han, Y., Kim, D., Hwang, G., Lee, B., Eom, I., Kim, J.P., Tong, M., Kim, H., 2014. Aggregation and dissolution of ZnO nanoparticles synthesized by different methods : Influence of ionic strength and humic acid. Colloids Surf. A 451, 7–15. http://dx.doi.org/10.1016/j.colsurfa.2014.03.030.
Handy, R.D., Shaw, B.J., 2007. Toxic effects of nanoparticles and nanomaterials: Implications for public health, risk assessment and the public perception of nanotechnology. Heal. Risk Soc. 9, 125–144. http://dx.doi.org/10.1080/13698570701306807.
Jahan, S., Yusoff, I. Bin, Alias, Y.B., Bakar, A.F.B.A., 2017. Reviews of the toxicity behavior of five potential engineered nanomaterials (ENMs) into the aquatic ecosystem. Toxicol. Rep. 4, 211–220. http://dx.doi.org/10.1016/j.toxrep.2017.04.001.
Jasper, A., Salih, H.H., Sorial, G.A., Sinha, R., Krishnan, R., Patterson, C.L., 2010. Impact of nanoparticles and natural organic matter on the removal of organic pollutants by activated carbon adsorption. Environ. Eng. Sci. 27, 85–93.
Jiang, Y., Yang, S., Liu, J., Ren, T., Zhang, Y., Sun, X., 2020. Degradation of hexabromocyclododecane (HBCD) by nanoscale zero-valent aluminum (nZVAl). Chemosphere 244, 125536. http://dx.doi.org/10.1016/j.chemosphere.2019.125536.
Kawaguchi, K., Kyuma, K., 1959. On the complex formation between soil humus and polyvalent cations. Soil Sci. Plant Nutr. 5, 54–63. http://dx.doi.org/10.1080/00380768.1959.10430895.
Khan, R., Inam, M.A., Khan, S., Park, D.R., Yeom, I.T., 2019. Interaction between persistent organic pollutants and ZnO NPs in synthetic and natural waters. Nanomaterials 9, 1–15. http://dx.doi.org/10.3390/nano9030472.
Khoshhesab, Z.M., Sarfaraz, M., Asadabad, M.A., 2011. Preparation of ZnO nanostructures by chemical precipitation method. Synth. React. Inorganic, Met. Nano-Metal Chem. 41, 814–819. http://dx.doi.org/10.1080/15533174.2011.591308.
Kodavanti, P.R.S., Loganathan, B.G., 2019. Polychlorinated biphenyls, polybrominated biphenyls, and brominated flame retardants. In: Biomarkers in Toxicology. Elsevier Inc., pp. 501–518. http://dx.doi.org/10.1016/B978-0-12-404630-6.00025-7.
Kodavanti, P.R.S., Stoker, T.E., Fenton, S.E., 2017. Brominated flame retardants. In: Reproductive and Developmental Toxicology. Elsevier Inc., pp. 681–710. http://dx.doi.org/10.1007/698.
Kodavanti, P.R.S., Szabo, D.T., Stoker, T.E., Fenton, S.E., 2011. Brominated flame retardants. In: Reproductive and Developmental Toxicology. Elsevier Inc., pp. 523–541. http://dx.doi.org/10.1016/B978-0-12-382032-7.10040-2.
Kroll, A., Behra, R., Kaegi, R., Sigg, L., 2014. Extracellular polymeric substances (EPS) of freshwater biofilms stabilize and modify CeO2 and Ag nanoparticles. PLoS One 9, 1–16. http://dx.doi.org/10.1371/journal.pone.0110709.
Lara, A.B., Caballo, C., Sicilia, M.D., Rubio, S., 2018. Speeding up the extraction of hexabromocyclododecane enantiomers in soils and sediments based on halogen bonding. Anal. Chim. Acta 1027, 47–56. http://dx.doi.org/10.1016/j.aca.2018.05.002.
Leareng, S.K., Jaswa, E.U., Musee, N., 2020. Toxicity of zinc oxide and iron oxide engineered nanoparticles to Bacillus subtilis in river water systems. Environ. Sci. Nano 7, 172–185. http://dx.doi.org/10.1039/c9en00585.
Lin, P.-C., Lin, S., Wang, P.C., Sridhar, R., 2014. Techniques for physicochemical characterization of nanomaterials. Biotechnol. Adv. 23, 1–39. http://dx.doi.org/10.1016/j.biotechadv.2013.11.006, Techniques.
Liu, Z., Bode, V., Hadayati, P., Onay, H., Sudhölter, E.J.R., 2020. Understanding the stability mechanism of silica nanoparticles: The effect of cations and EOR chemicals. Fuel 280, 118650. http://dx.doi.org/10.1016/j.fuel.2020.118650.
Liu, T., Zhang, Y., Hou, J., Lu, S., Jiang, J., Xu, M., 2015. High performance mesoporous C@Se composite cathodes derived from Ni-based MOFs for Li-Se batteries. RSC Adv. 5, 84038–84043. http://dx.doi.org/10.1039/c5ra14979g.
Lu, S., Tan, Z., Jiang, Y., Wu, D., Zhang, J., Zhou, J., Lin, X., 2018. Hexabromocyclododecanes in breast milk from residents in Shenzhen, China: Implications for infant exposure. Sci. Total Environ. 622–623, 1090–1097. http://dx.doi.org/10.1016/j.scitotenv.2017.11.277.
MacCuspie, R.I., 2011. Colloidal stability of silver nanoparticles in biologically relevant conditions. J. Nanoparticle Res. 13, 2893–2908. http://dx.doi.org/10.1007/s11051-010-0178-x.
Majedi, S.M., Kelly, B.C., Lee, H.K., 2014. Role of combinatorial environmental factors in the behavior and fate of ZnO nanoparticles in aqueous systems: A multiparametric analysis. J. Hazard. Mater. 264, 370–379. http://dx.doi.org/10.1016/j.jhazmat.2013.11.015.

Marvin, C.H., Tomy, G.T., Armitage, J.M., Arnot, J.A., McCarty, L., Covaci, A., Palace, V., 2011. Hexabromocyclododecane: Current understanding of chemistry, environmental fate and toxicology and implications for global management. Environ. Sci. Technol. 45, 8613–8623. http://dx.doi.org/10.1021/es201548c.
McCall, M.J., Gulson, B., Andrews, D., 2018. Consumer use of sunscreens containing nanoparticles. In: Nanotechnology Environmental Health and Safety. Elsevier Inc., http://dx.doi.org/10.1016/b978-0-12-813588-4.00016-6.
Mohd Omar, F., Abdul Aziz, H., Stoll, S., 2014. Aggregation and disaggregation of ZnO nanoparticles: influence of pH and adsorption of Suwannee River humic acid. Sci. Total Environ. 468–469, 195–201. http://dx.doi.org/10.1016/j.scitotenv.2013.08.044.
Nowack, B., Bucheli, T.D., 2007. Occurrence, behavior and effects of nanoparticles in the environment. Environ. Pollut. 150, 5–22. http://dx.doi.org/10.1016/j.envpol.2007.06.006.
Okonski, K., Melymuk, L., Kohoutek, J., Klánová, J., 2018. Hexabromocyclododecane: concentrations and isomer profiles from sources to environmental sinks. Environ. Sci. Pollut. Res. 25, 36624–36635. http://dx.doi.org/10.1007/s11356-018-3381-4.
Park, C.M., Chu, K.H., Her, N., Jang, M., Baalousha, M., Heo, J., Yoon, Y., 2017. Occurrence and removal of engineered nanoparticles in drinking water treatment and wastewater treatment processes. Sep. Purif. Rev. 46, 255–272. http://dx.doi.org/10.1080/15422119.2016.1260588.
Peng, Y., Tsai, Y., Hsiung, C., Lin, Y., Shih, Y., 2017. Influence of water chemistry on the environmental behaviors of commercial ZnO nanoparticles in various water and wastewater samples. J. Hazard. Mater. 322, 348–356. http://dx.doi.org/10.1016/j.jhazmat.2016.10.003.
Philippe, A., Schaumann, G.E., 2014. Interactions of dissolved organic matter with natural and engineered inorganic colloids: A review. Environ. Sci. Technol. 48, 8946–8962. http://dx.doi.org/10.1021/es502342r.
Pudukudy, M., Yaakob, Z., 2015. Facile synthesis of quasi spherical ZnO nanoparticles with excellent photocatalytic activity. J. Clust. Sci. 26, 1187–1201. http://dx.doi.org/10.1007/s10876-014-0806-1.
Quigg, A., Chin, W.C., Chen, C.S., Zhang, S., Jiang, Y., Miao, A.J., Schwehr, K.A., Xu, C., Santschi, P.H., 2013. Direct and indirect toxic effects of engineered nanoparticles on algae: Role of natural organic matter. ACS Sustain. Chem. Eng. 1, 686–702. http://dx.doi.org/10.1021/sc400103x.
Rajput, V.D., Minkina, T.M., Behal, A., Sushkova, S.N., Mandzhieva, S., Singh, R., Gorovtsov, A., Tsitsuashvili, V.S., Purvis, W.O., Ghazaryan, K.A., Movsesyan, H.S., 2018. Effects of zinc-oxide nanoparticles on soil, plants, animals and soil organisms : A review. Environ. Nanotechnology Monit. Manag. 9, 76–84. http://dx.doi.org/10.1016/j.enmm.2017.12.006.
Santos, A.M.P., Bertoli, A.C., Borges, A.C.C.P., Gomes, R.A.B., Garcia, J.S., Trevisan, M.G., 2018. New organomineral complex from humic substances extracted from poultry wastes: Synthesis, characterization and controlled release study. J. Braz. Chem. Soc. 29, 140–150. http://dx.doi.org/10.21577/0103-5053.20170122.
Schneider, S.L., Lim, H.W., 2019. A review of inorganic UV filters zinc oxide and titanium dioxide. Photodermatol. Photoimmunol. Photomed. 35, 442–446. http://dx.doi.org/10.1111/phpp.12439.
Senapati, S., Srivastava, S.K., Singh, S.B., 2012. Synthesis, characterization and photocatalytic activity of magnetically separable hexagonal Ni/ZnO nanostructure. Nanoscale 4, 6604–6612. http://dx.doi.org/10.1039/c2nr31831h.
Sharma, V.K., Sayes, C.M., Guo, B., Pillai, S., Parsons, J.G., Wang, C., Yan, B., Ma, X., 2019. Interactions between silver nanoparticles and other metal nanoparticles under environmentally relevant conditions: A review. Sci. Total Environ. 653, 1042–1051. http://dx.doi.org/10.1016/j.scitotenv.2018.10.411.
Song, R., Qin, Y., Suh, S., Keller, A.A., 2017. Dynamic model for the stocks and release flows of engineered nanomaterials. Environ. Sci. Technol. 51, 12424–12433. http://dx.doi.org/10.1021/acs.est.7b01907.
Stuart, B.H., 2004. Infrared spectroscopy: Fundamentals and applications. In: Infrared Spectroscopy: Fundamentals and Applications. pp. 1–224. http://dx.doi.org/10.1002/0470011149.
Studart, A.R., Amstad, E., Gauckler, L.J., 2007. Colloidal stabilization of nanoparticles in concentrated suspensions. Langmuir 23, 1081–1090. http://dx.doi.org/10.1021/la062042s.
Sudiono, S., Yuniarti, M., Siswanta, D., Kunarti, E.S., Triyono, Santosa, S.J., 2017. The role of carboxyl and hydroxyl groups of humic acid in removing AuCl4- from aqueous solution. Indones. J. Chem. 17, 95–104. http://dx.doi.org/10.22146/ijc.23620.
Talam, S., Karumuri, S.R., Gunnam, N., 2012. Synthesis, characterization, and spectroscopic properties of ZnO nanoparticles. ISRN Nanotechnol. 2012, 1–6. http://dx.doi.org/10.5402/2012/372505.
Tambo, N., Hozumi, H., 1979. Physical characteristics of flocs-II. Strength Floc. Water Res. 13, 421–427.
Thio, B.J.R., Zhou, D., Keller, A.A., 2011. Influence of natural organic matter on the aggregation and deposition of titanium dioxide nanoparticles. J. Hazard. Mater. 189, 556–563. http://dx.doi.org/10.1016/j.jhazmat.2011.02.072.
Waaijers, S.L., Parsons, J.R., 2016. Biodegradation of brominated and organophosphorus flame retardants. Curr. Opin. Biotechnol. 38, 14–23. http://dx.doi.org/10.1016/j.copbio.2015.12.005.
Wang, X., Adeleye, A.S., Wang, H., Zhang, M., Liu, M., Wang, Y., Li, Y., Keller, A.A., 2018. Interactions between polybrominated diphenyl ethers (PBDEs) and TiO2 nanoparticle in artificial and natural waters. Water Res. 146, 98–108. http://dx.doi.org/10.1016/j.watres.2018.09.019.
Wang, F., Yao, J., Chen, H., Yi, Z., Xing, B., 2013. Sorption of humic acid to functionalized multi-walled carbon nanotubes. Environ. Pollut. 180, 1–6. http://dx.doi.org/10.1016/j.envpol.2013.04.035.
Westerhoff, P., Song, G., Hristovski, K., Kiser, M.A., 2011. Occurrence and removal of titanium at full scale wastewater treatment plants: Implications for TiO2 nanomaterials. J. Environ. Monit. 13, 1195–1203. http://dx.doi.org/10.1039/c1em10017c.
Wilkinson, J., Hooda, P.S., Barker, J., Barton, S., Swinden, J., 2017. Occurrence, fate and transformation of emerging contaminants in water: An overarching review of the field. Environ. Pollut. 231, 954–970. http://dx.doi.org/10.1016/j.envpol.2017.08.032.
Wong, S.W.Y., Zhou, G.J., Leung, P.T.Y., Han, J., Lee, J.S., Kwok, K.W.H., Leung, K.M.Y., 2020. Sunscreens containing zinc oxide nanoparticles can trigger oxidative stress and toxicity to the marine copepod Tigriopus japonicus. Mar. Pollut. Bull. 154, 111078. http://dx.doi.org/10.1016/j.marpolbul.2020.111078.
Xiao, X., Chen, B., 2016. Interaction mechanisms between biochar and organic pollutants. Agric. Environ. Appl. Biochar Adv. Barriers 63, 225–257. http://dx.doi.org/10.2136/sssaspecpub63.2014.0044.
Yamabi, S., Imai, H., 2002. Growth conditions for wurtzite zinc oxide films in aqueous solutions. J. Mater. Chem. 12, 3773–3778. http://dx.doi.org/10.1039/b205384e.
Yi, X., Zhang, K., Han, G., Yu, M., Chi, T., Jing, S., Li, Z., Zhan, J., Wu, M., 2018. Toxic effect of triphenyltin in the presence of nano zinc oxide to marine copepod Tigriopus japonicus. Environ. Pollut. 243, 687–692. http://dx.doi.org/10.1016/j.envpol.2018.09.038.
Yu, S., Liu, J., Yin, Y., Shen, M., 2018. Interactions between engineered nanoparticles and dissolved organic matter: A review on mechanisms and environmental effects. J. Environ. Sci. (China) 63, 198–217. http://dx.doi.org/10.1016/j.jes.2017.06.021.
Zak, A.K., Razali, R., Majid, W.H.A., Darroudi, M., 2011. Synthesis and characterization of a narrow size distribution of zinc oxide nanoparticles. Int. J. Nanomedicine 6, 1399–1403. http://dx.doi.org/10.2147/ijn.s19693.
Zhang, K., Huang, J., Wang, H., Liu, K., Yu, G., Deng, S., Wang, B., 2014. Mechanochemical degradation of hexabromocyclododecane and approaches for the remediation of its contaminated soil. Chemosphere 116, 40–45. http://dx.doi.org/10.1016/j.chemosphere.2014.02.006.
Zhang, X., Servos, M.R., Liu, J., 2012. Ultrahigh nanoparticle stability against salt, pH and solvent with retained surface accessibility via depletion stabilization. J. Am. Chem. Soc. 134, 9910–9913.
Zhang, C., Wang, J., Tan, L., Chen, X., 2016. Toxic effects of nano-ZnO on marine microalgae Skeletonema costatum: Attention to the accumulation of intracellular Zn. Aquat. Toxicol. 178, 158–164. http://dx.doi.org/10.1016/j.aquatox.2016.07.020.